DEVELOPMENTAL NEUROSCIENCE

A Zic2-regulated switch in a noncanonical Wnt/βcatenin pathway is essential for the formation of bilateral circuits

Cruz Morenilla-Palao, María Teresa López-Cascales, José P. López-Atalaya, Diana Baeza, Luís Calvo-Díaz, Angel Barco, Eloísa Herrera*

The Wnt pathway is involved in a wide array of biological processes during development and is deregulated in many pathological scenarios. In neurons, Wnt proteins promote both axon extension and repulsion, but the molecular mechanisms underlying these opposing axonal responses are unknown. Here, we show that Wnt5a is expressed at the optic chiasm midline and promotes the crossing of retinal axons by triggering an alternative Wnt pathway that depends on the accumulation of βcatenin but does not activate the canonical pathway. In ipsilateral neurons, the transcription factor Zic2 switches this alternative Wnt pathway by regulating the expression of a set of Wnt receptors and intracellular proteins. In combination with this alternative Wnt pathway, the asymmetric activation of EphB1 receptors at the midline phosphorylates βcatenin and elicits a repulsive response. This alternative Wnt pathway and its Zic2-triggered switch may operate in other contexts that require a two-way response to Wnt ligands.

INTRODUCTION

To establish neuronal connectivity in the adult brain, neurons located far from their targets must extend an axon that navigates over long distances during embryonic development to reach the target tissue. Using simple models such as the axonal binary decision of crossing or not the midline in vertebrates or invertebrates, different families of secreted (Netrin and Slits) and membrane (Eph/ephrins) proteins were initially identified as axon guidance molecules (*1*–*3*). Later, the highly conserved proteins Wnts—originally described as key regulators of body axis patterning, cell fate specification, proliferation, cell migration, and carcinogenesis—were found to be also involved in axon guidance and mediate both attractive and repulsive responses in different contexts. For instance, while Wnt5 repels ventral nerve axons expressing the Derailed receptor in *Drosophila* (*4*, *5*), vertebrate post-commissural axons are attracted by Wnts (*6*).

Intracellularly, Wnt signaling is a particularly complex pathway that leads to the activation of two main alternative branches: the canonical and the noncanonical pathway, with the latter, in turn, being divided into the planar cell polarity (PCP) and calcium pathways. This classification relies on the participation of βcatenin, an important intracellular signal transducer that links the membrane adhesion protein E-cadherin to the actin cytoskeleton (*7*). In the absence of Wnt, free cytosolic βcatenin is constantly degraded by the destruction complex formed by GSK3, Axin, and Apc (Apc2 in the nervous system). In the canonical pathway, the binding of Wnt proteins to their receptors (Frizzled and Lrp5/6) triggers the inactivation or disassembly of the destruction complex, which reduces βcatenin phosphorylation and promotes its accumulation and translocation to the nucleus. There, βcatenin forms a complex with Lef/Tcf factors and induces the transcription of specific genes. In contrast, activation of the noncanonical pathway does not depend on βcatenin-driven transcription; instead, it relies on changes that affect cytoskeletal organization and calcium homeostasis (*8*). The role of classical PCP proteins in polarizing epithelial tissues made the noncanonical branch the most likely candidate to translate Wnt signals into the polarization of the motile axon growth cone. Consistent with this view, mutant mice for typical PCP receptors such as Celsr3 (cadherin EGF LAG seven-pass G-type receptor 3, also known as Flamingo) or Vangl2 (Van Gogh–like protein 2) exhibit pathfinding defects in the ascending and descending projections of the brainstem, in the longitudinal axis of the spinal cord, and in other fiber tracts (*9*–*12*). However, more recent studies have shown that manipulation of different components of the canonical pathway, including βcatenin, alters axon midline behavior in the chick spinal cord (*13*). This, along with studies showing that Wnt5a may act as an activator of the canonical pathway (*14*), has challenged the idea of PCP as the only Wnt signaling branch involved in guidance. Therefore, the mechanisms by which Wnt proteins mediate axon attraction or repulsion and the branch of the Wnt pathway involved in axon guidance remain unclear.

In the developing visual system, retinal ganglion cells (RGCs) projecting ipsilaterally (iRGCs) are located in the peripheral ventrotemporal retina and contralaterally projecting ganglion cells (cRGCs) distribute in the remainder retina. The spatial segregation of iRGCs and cRGCs facilitates their genetic manipulation and the labeling and visualization of individual axons when they are crossing or avoiding the midline. By using this binary system, here, we disentangle some of the unknown mechanisms underlying Wnt signaling pathways during axon guidance decisions. We first demonstrate that cRGC and iRGC axons transduce Wnt5a signaling differentially. In contralateral neurons, a previously unidentified form of Wnt signaling that depends on accumulation of βcatenin but is noncanonical is activated to promote midline crossing. In ipsilateral axons, the positive response to Wnt5a is switched off by Zic2, a transcription factor (TF) previously described as the determinant of ipsilateral identity and known to induce the expression of the tyrosine kinase receptor EphB1 (*15*–*17*). Then, we identified the set of Zic2-regulated genes

Instituto de Neurociencias, Consejo Superior de Investigaciones Científicas-Universidad Miguel Hernández (CSIC-UMH), Campus San Juan, Av. Ramón y Cajal s/n, Alicante 03550, Spain.
*Corresponding author. Email: e.herrera@umh.es

that blocks the positive response to Wnt5a, and show that a concomitant asymmetric activation of EphB1 at the growth cone would mediate phosphorylation of βcatenin to trigger actin filament destabilization to facilitate axon steering.

RESULTS

Wnt5a enhances the growth of contralaterally projecting axons

Wnt signaling is known to play an important role in axonal navigation in different contexts and species, but its function in the guidance of visual axons at the midline has not been explored. To assess the role of Wnt signaling in the navigation of retinal axons, we first analyzed the expression of different members of the Wnt family at the optic chiasm by in situ hybridization. Among the different Wnts expressed at the chiasm region (fig. S1), we detected *Wnt5a mRNA* at the midline in a spatiotemporal pattern that resembles that of ephrinB2 (Fig. 1A), a repulsive guidance molecule expressed by glial cells that induces the turning of iRGCs (*18*). We noticed that contrasting to other Wnt proteins that have been reported as expressed in the ciliary margin zone of the eye (*19*, *20*), *Wnt5a mRNA* is not expressed in the retina (fig. S1). This result points toward Wnt5a as a candidate to influence axon guidance at the midline.

To investigate whether Wnt5a has an effect on RGC axons, explants from the central retina of E14.5 mouse embryos that contain contralaterally but not ipsilaterally projecting neurons were cultured for 12 hours in the presence of Wnt5a. The axons from explants cocultured with Wnt5a extended significantly longer axons than those not exposed to Wnt5a (Fig. 1, B to D), indicating that RGC axons respond positively to Wnt5a. In addition, acute exposure to Wnt5a leads to a significant increase in the size of the growth cone and in the levels of βcatenin (Fig. 1, E to G).

A noncanonical but βcatenin-dependent branch of the Wnt pathway mediates midline crossing

Then, to investigate the participation of βcatenin in midline crossing, we down-regulated βcatenin in RGCs at the time that the majority of visual axons are crossing the midline. Short hairpin RNA against βcatenin (ctnnb1 shRNA) (fig. S2) was injected and electroporated into the retinas of E13.5 mouse embryos, and the axonal projection phenotype of targeted neurons at the optic chiasm was analyzed 5 days later. As a control, retinas were also electroporated with plasmids bearing random shRNAs. In addition, plasmids encoding enhanced green fluorescent protein (EGFP) were co-injected in both cases to visualize the axons of targeted neurons at the chiasm. In embryos electroporated with control shRNAs, the large majority of the axons crossed the midline. However, embryos electroporated with ctnnb1 shRNA plasmids showed strongly altered axonal trajectories at the chiasm. The majority of the RGC fibers exited the retina (fig. S2), but a large number of them stalled at the midline and a subset aberrantly grew into the ipsilateral path (Fig. 2, A and B). To explore whether this phenotype may be caused by an axonal incapacity to respond to Wnt5a, we challenged retinal explants electroporated with control or ctnnb1 shRNAs with Wnt5a. Ctnnb1 shRNAs axons from explants incubated with the vehicle showed a modest defect in axon growth compared to axons from control shRNA–electroporated explants, as expected for a protein involved in adhesion and linked to cadherins (*21*). Axons with reduced levels of βcatenin did not show enhanced growth after incubation with Wnt5a (Fig. 2, C and D), suggesting that the stalling phenotype of axons with ctnnb1 shRNAs observed at the midline is a consequence of their incapacity to respond to Wnt5a.

The effects of Wnt5a treatment and the phenotype obtained after knocking down βcatenin on cRGCs were suggesting that contralateral neurons could be activating the canonical pathway while confronting Wnt5a at the chiasm. To test this hypothesis, we electroporated retinas from E13.5 embryos with a reporter plasmid for canonical Wnt signaling (referred to as Top-RFP) that contains several TCF/LEF (T cell factor/lymphoid enhancer factor) binding sites upstream of the coding sequence of the red fluorescence protein (RFP) (*22*). As a positive control, we used an N-terminal–truncated form of βcatenin (Δ90βcat) that lacks phosphorylation sites responsible for its degradation and therefore accumulates intracellularly and promotes βcatenin-dependent transcription (*23*). Retinas from embryos electroporated with Top-RFP plus Δ90βcat expressed high levels of RFP 2 days later. However, no red signal was detected in retinas electroporated with Top-RFP alone (Fig. 2E), indicating that although βcatenin is required for midline crossing, canonical Wnt signaling is not active in RGCs when the axons are crossing the chiasm.

Zic2 silences the positive response to Wnt5a in ipsilateral RGCs

We demonstrated that Wnt5a enhances the growth of contralateral axons and triggers local accumulation of βcatenin at the tip of the growth cone. What about ipsilateral axons? Do they also respond to Wnt5a? To address this question, we analyzed the response of ipsilateral axons to Wnt5a by using the Sert-RFP mouse line in which iRGCs are labeled with the RFP (Materials and Methods) (*24*, *25*). Retinal explants isolated from E14 Sert-RFP embryos were grown for 12 hours and incubated with Wnt5a or a vehicle for 1 hour. In contrast to RFP axons exposed to the vehicle, most RFP axons collapsed upon exposure to Wnt5a (Fig. 3, A and B), revealing that contralateral and ipsilateral axons respond differentially to Wnt5a. Because the TF Zic2 determines axon midline avoidance in iRGCs (*15*, *16*), we wondered whether Zic2 underlies the differential response of iRGC and cRGC axons to Wnt5a. To address this question, retinal explants from embryos electroporated with Zic2 and EGFP or EGFP alone were plated on dishes and incubated with Wnt5a for 12 hours (Fig. 3C). As expected, the axons of EGFP-electroporated explants (controls) extended significantly longer axons in the presence of Wnt5a than with the vehicle (Fig. 3C). In contrast, the axons from Zic2-expressing explants did not exhibit enhanced growth after Wnt5a treatment (Fig. 3D), indicating that Zic2 is able to modify the positive response of contralateral axons to Wnt5a. Moreover, the acute exposure of Zic2-expressing neurons to Wnt5a resulted in a significant increase of collapsing axons compared to controls (Fig. 3, E and F). These results strongly suggested that the negative response of iRGCs to Wnt5a is controlled by Zic2.

Zic2 regulates many genes related to the Wnt signaling pathway

Our results show that cRGCs and RGCs expressing Zic2 respond differentially to Wnt5a, suggesting that Zic2 must control some genes related to the Wnt pathway. To address this question, we analyzed the genetic program activated by Zic2 in an unbiased manner by comparing the transcriptomic profiles of RGCs expressing or not Zic2. Retinas from E13.5 embryos electroporated with Zic2 and EGFP plasmids or with EGFP plasmids alone were isolated, and EGFP

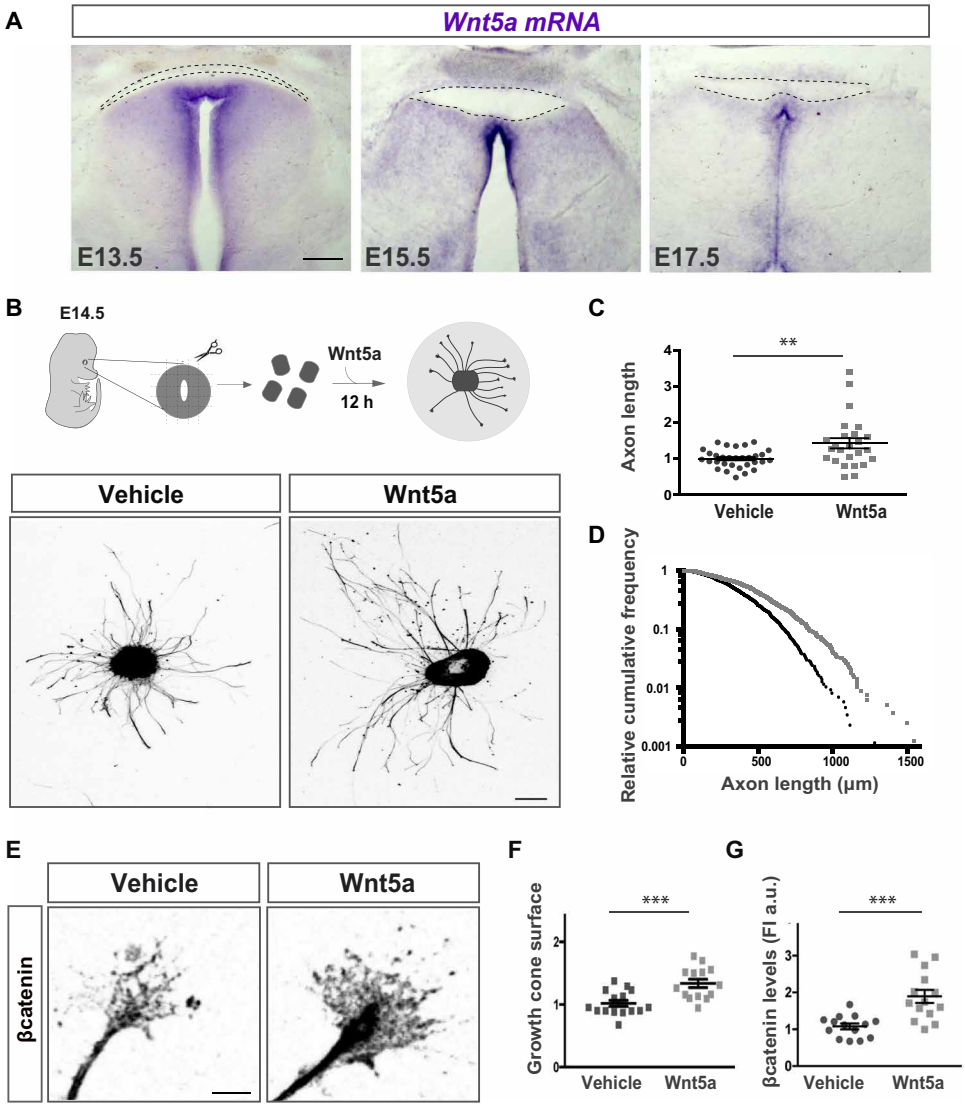

Fig. 1. Wnt5A is expressed at the midline and enhances axonal growth of contralateral axons. (**A**) In situ hybridization for Wnt5a in coronal sections from E13.5, E15.5, and E17.5 embryos. Scale bar, 200 μm. (**B**) Color-inverted Tuj1 staining on retinal explants from E14.5 embryos cultured for 12 hours. Retinal explants from the central retina treated with recombinant Wnt5a protein display longer neurites compared with vehicle-treated explants. Scale bar, 100 μm. (**C**) Quantification of average axon length in explants treated with vehicle or Wnt5a (*n* = mean length of axons/explant). Data from three biological replicates. Two-tailed Mann-Whitney *U* test, $^{**}P < 0.01$. (**D**) Relative cumulative frequency histogram showing axonal length in explants growing in the presence of Wnt5a (gray; *n* = 927) or the vehicle (black; *n* = 861). Each dot represents an individual neurite. *n* = number of axons from three biological replicates. (**E**) Color-inverted immunohistochemistry for βcatenin in the growth cone of ganglion cells from contralateral axons treated for 1 hour with Wnt5a or vehicle. Note that Wnt5a-treated cones occupy a larger area and show higher levels of βcatenin. Scale bar, 5 μm. (**F** and **G**) Quantification of growth cone area and βcatenin fluorescence intensity (FI) in retinal explants. *n* = mean from at least four growth cones/explant. Results from three independent experiments. βCatenin levels (two-tailed Mann-Whitney *U* test). Growth cone area (two-tailed unpaired *t* test, $^{***}P < 0.001$). Results show means ± SEM. a.u., arbitrary units.

cells were sorted by flow cytometry 36 hours after electroporation and compared by RNA sequencing (RNA-seq) analysis (Fig. 4A and fig. S3A). This mRNA-seq screen identified 423 up-regulated genes and 192 down-regulated genes ($P_{adj} < 0.1$) (Fig. 4B). As expected, Zic2 was the most up-regulated gene in the cells electroporated with Zic2-encoding plasmids (fig. S3B). Genes encoding for the tyrosine receptor EphB1 and the serotonin transporter Sert, previously described as Zic2 targets (*17*, *24*), were also up-regulated (fig. S3C). In addition, Zic2 expression strongly down-regulated Sox4, a TF that promotes cRGC differentiation and axonal midline crossing (*26*) as well as Brn3a and Isl2, which have been reported to be expressed in contralaterally but not in ipsilaterally projecting neurons (fig. S3D) (*27*, *28*). In addition to all the already known Zic2 targets, we identified an important number of genes related to the Wnt pathway in a PANTHER (protein analysis through evolutionary relationship) pathways analysis (Fig. 4C). Gene set enrichment analysis (GSEA) confirmed the important impact of Zic2 expression on Wnt pathway genes, and a heatmap analysis focused on the Wnt pathway revealed that Zic2 induces the expression of genes encoding for specific Wnt receptors such as *Fzd1*, *Fzd8*, or *Lgr5*. Although no changes were

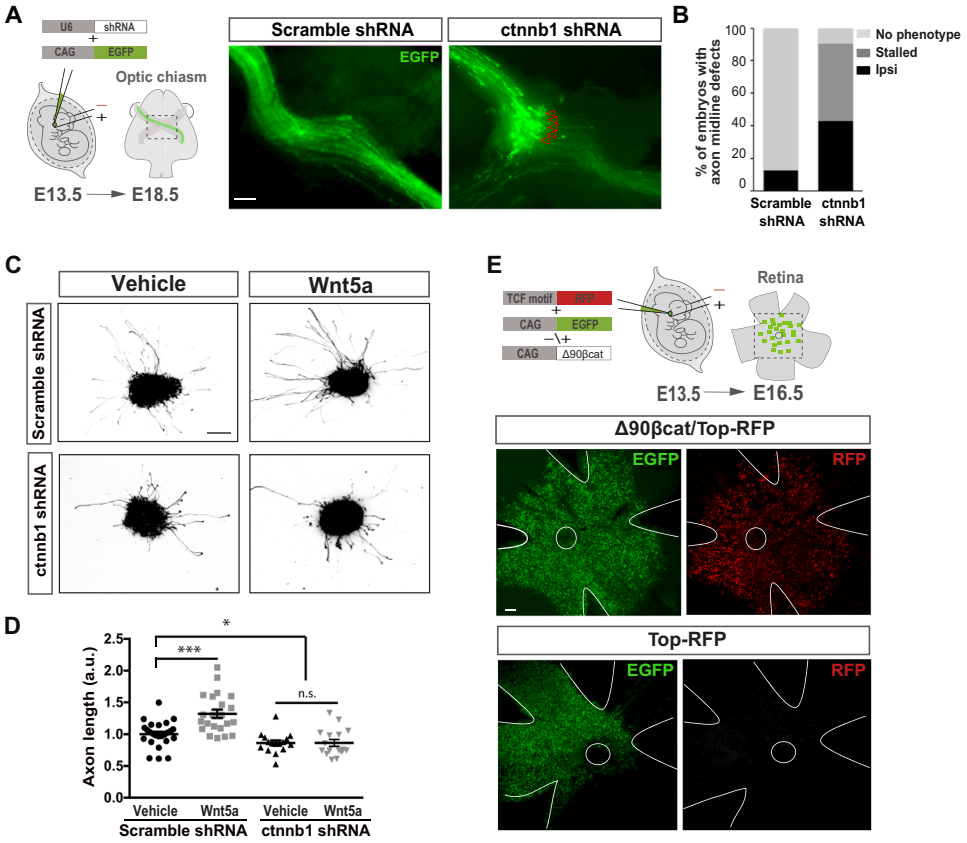

Fig. 2. βCatenin is necessary for midline crossing. (**A**) Plasmids encoding EGFP and control shRNA or shRNA against βcatenin (ctnnb1 shRNAs) were electroporated into one eye of E13.5 embryos, and EGFP axons into the optic chiasm were analyzed at E18.5. Right panels are representative images of optic chiasms from embryos electroporated with ctnnb1 shRNA or scramble shRNA plasmids. Down-regulation of βcatenin in contralaterally projecting neurons inhibits midline crossing. Scale bar, 100 μm. (**B**) Graph represents the percent of embryos showing midline crossing defects after electroporation with scramble shRNAs [n = 10; no phenotype (NP) = 87.5%; ectopic ipsilateral projection (Ipsi) = 12.5%] or ctnnb1 shRNAs (n = 42; NP = 9.52%; Ipsi = 42.86%; and stalled = 47.62%) plasmids. (**C**) Color-inverted images of retinal explants from E14 embryos electroporated with ctnnb1 shRNAs plus EGFP plasmids or with control shRNA plus EGFP plasmids cultured for 12 hours with Wnt5a or vehicle. Scale bar, 100 μm. (**D**) Axon length quantification of control and ctnnb1 shRNAs cultured with Wnt5a or vehicle, as in (C). n = mean length of axons/explant. Results from three independent experiments. Two-tailed unpaired t test (*P < 0.05 and ***P < 0.001). Results show means ± SEM. n.s., not significant. (**E**) Representative immunohistochemistry for RFP and EGFP in whole-mount E16.5 retinas that electroporated at E13.5 with Top-RFP– and EGFP-encoding or Δ90-βCatenin/Top-RFP– and EGFP-encoding plasmids shows that canonical Wnt signaling is not activated in cRGCs at the time that visual axons transverse the midline. The experiment was repeated at least three times for each condition with similar results. Scale bar, 100 μm.

detected in the Zic2 samples in *Fzd3*, *Fzd5*, or *Ryk* transcripts, we observed that they were highly expressed in the GFP samples, suggesting that they could be the receptors mediating the positive response to Wnt5a in cRGCS (fig. S3F). Other components of the Wnt pathway such as the adenomatous polyposis coli protein 2 (Apc2) were down-regulated in Zic2-expressing neurons (Fig. 4, C to E). Thus, this genome-wide analysis underscored a strong link between Zic2 and the Wnt pathway during axon midline avoidance and revealed the set of genes regulated by Zic2 during this process.

The gene network triggered by Zic2 induces βcatenin accumulation

To validate the RNA-seq analysis, we analyzed the expression of some of the candidates by performing in situ hybridization and immunostaining in retinal sections. In situ hybridization for one of the Wnt receptors identified in the RNA-seq screen (*Fzd8*) demonstrated that this Wnt receptor has a restricted expression in the ventrotemporal retina, coinciding with the position of iRGCs (Fig. 5A) and consistent with the idea that Zic2 endogenously regulates these Wnt receptors. We also confirmed the down-regulation of Apc2 in the growth cone of RGCs ectopically expressing Zic2 by immunostaining (Fig. 5, B and C), in line with previous studies suggesting that Apc regulates axon behavior and is required for midline crossing (*29*, *30*). Consistent with the known role of Apc2 as an integrant of the βcatenin degradation complex, we also observed a significant and homogeneous accumulation of βcatenin in the cones of Zic2-expressing RGCs (Fig. 5, B and C). These results indicated that although *Ctnnb1* (the gene encoding βcatenin) transcription is not directly affected by Zic2 (fig. S3E), the presence of this TF indirectly regulates the levels of βcatenin and produces an accumulation of this protein in the neuron. This accumulation of βcatenin did not activate, however, the canonical pathway, as electroporation of Top-RFP plasmids in Zic2 neurons did not result in RFP expression. Retinas electroporated with Zic2, Top-RFP, and Δ90βcat plasmids showed a significant reduction in RFP expression compared to the control (Fig. 5, D and E), indicating that in this artificial scenario, instead of inducing canonical Wnt

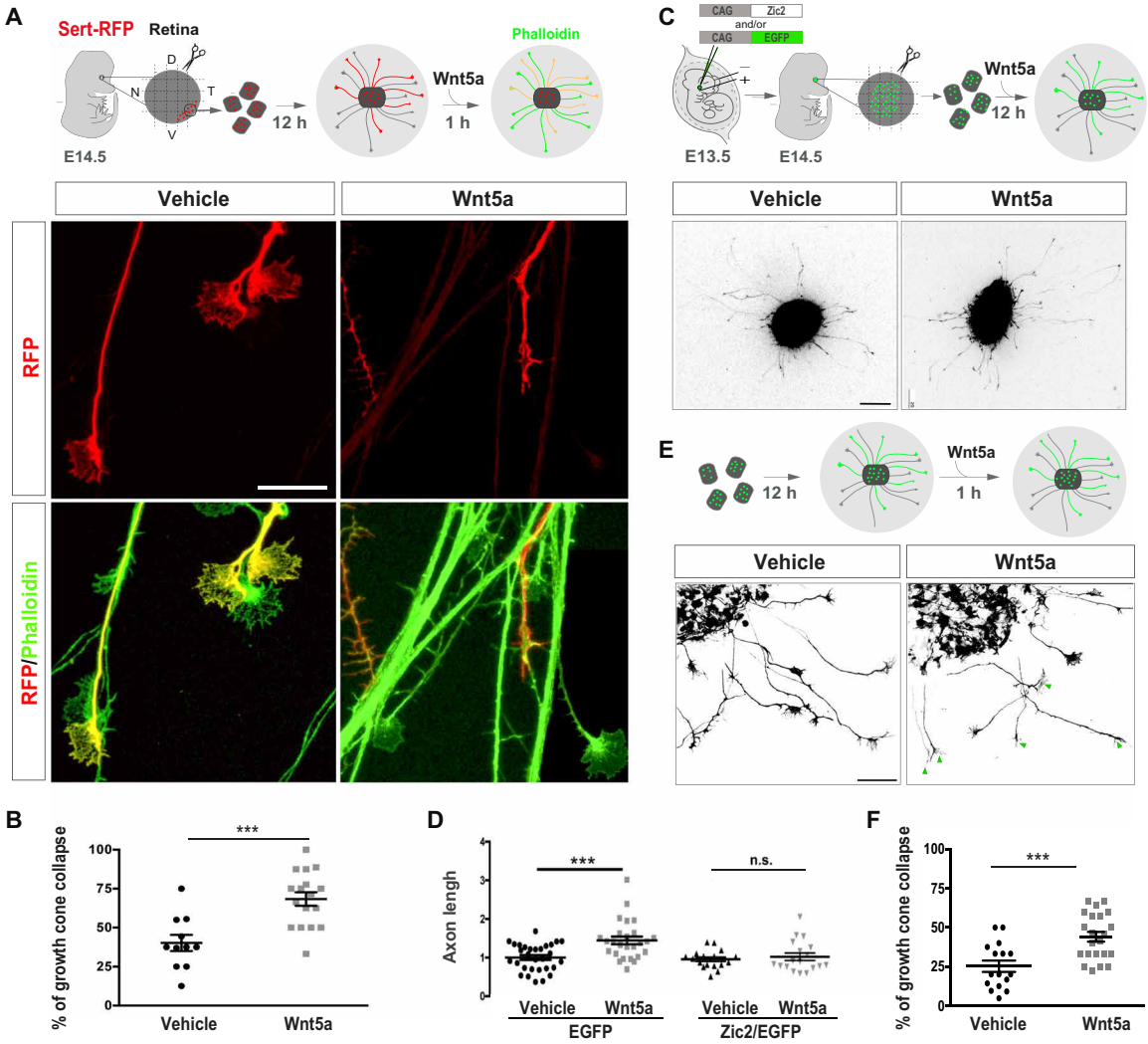

Fig. 3. Ipsilateral RGC axons collapse in response to Wnt5a. (**A**) Top panel shows the experimental approach used to assess the response of ipsilateral RGCs to Wnt5a. (Bottom) Retinal explants from Sert-RFP E15 embryos cultured for 12 hours, incubated with vehicle or Wnt5a for 1 hour, and stained with phalloidin. Scale bar, 20 μm. (**B**) Quantification showing the percentage of growth cones smaller than 70 μm (% collapse) in Sert-RFP explants incubated with Wnt5a or the vehicle. Results from three independent experiments. Two-tailed unpaired *t* test (***$P < 0.001$). Results show means ± SEM. (**C**) Top panels show the experimental approach used to assess the response of Zic2-expressing neurons to Wnt5a. Color-inverted retinal explants from E14.5 embryos electroporated at E13.5 with EGFP- or Zic2/EGFP-encoding plasmids were isolated and cultured with or without Wnt5a. The bottom images are retinal explants from electroporated embryos incubated with Wnt5a or vehicle. Scale bar, 200 μm. (**D**) Quantification of axonal length of RGCs expressing EGFP or Zic2/EGFP grown in the presence of Wnt5a or vehicle (*n* = number of explants). Axon length values were normalized to the mean value of the axons in explants treated with the vehicle. Results from three independent experiments. Two-tailed unpaired *t* test, $P = 0.003$ (EGFP) and $P = 0.563$ (Zic2). (**E**) Schema summarizing the experimental approach. Color-inverted images show axons from representative retinal explants isolated from electroporated embryos that were cultured for 12 hours and exposed to Wnt5a or vehicle for 1 hour. Green arrowheads point out axons with growth cones smaller than 70 μm. Scale bar, 50 μm. (**F**) Quantification showing the percentage of collapsed growth cones in Zic2-expressing explants incubated with Wnt5a or the vehicle. *n* = mean length of axons/explant (two-tailed unpaired *t* test, ***$P < 0.001$). Results from three independent experiments. Results show means ± SEM.

signaling, Zic2 is able to inhibit this pathway, which was also consistent with the observation that En2, a TF involved in the nuclear translocation of βcatenin (*31*), is down-regulated upon Zic2 expression (fig. S3).

Our results have shown that down-regulation of βcatenin in contralateral neurons provokes stalling at the midline, while in ipsilateral neurons, Zic2 induces accumulation of βcatenin. These results inspired the idea that polarized accumulation of βcatenin at the tip of the growth cone induced by Wnt5a is essential for crossing and disturbing this polarization could disrupt midline crossing. To address this hypothesis, we analyzed E16.5 embryos electroporated at E13.5 with plasmids encoding either wild-type (WT) βcatenin or a variant form of this protein that is resistant to Apc2-mediated degradation and also lacks the transactivation domain (ΔCT-βcat). The chiasm of embryos electroporated with WT βcatenin plasmids was undistinguishable from the controls electroporated with EGFP-encoding plasmids alone. However, forced unpolarized accumulation of βcatenin achieved by the expression of this nondegradable truncated protein leads to a nearly random projection phenotype,

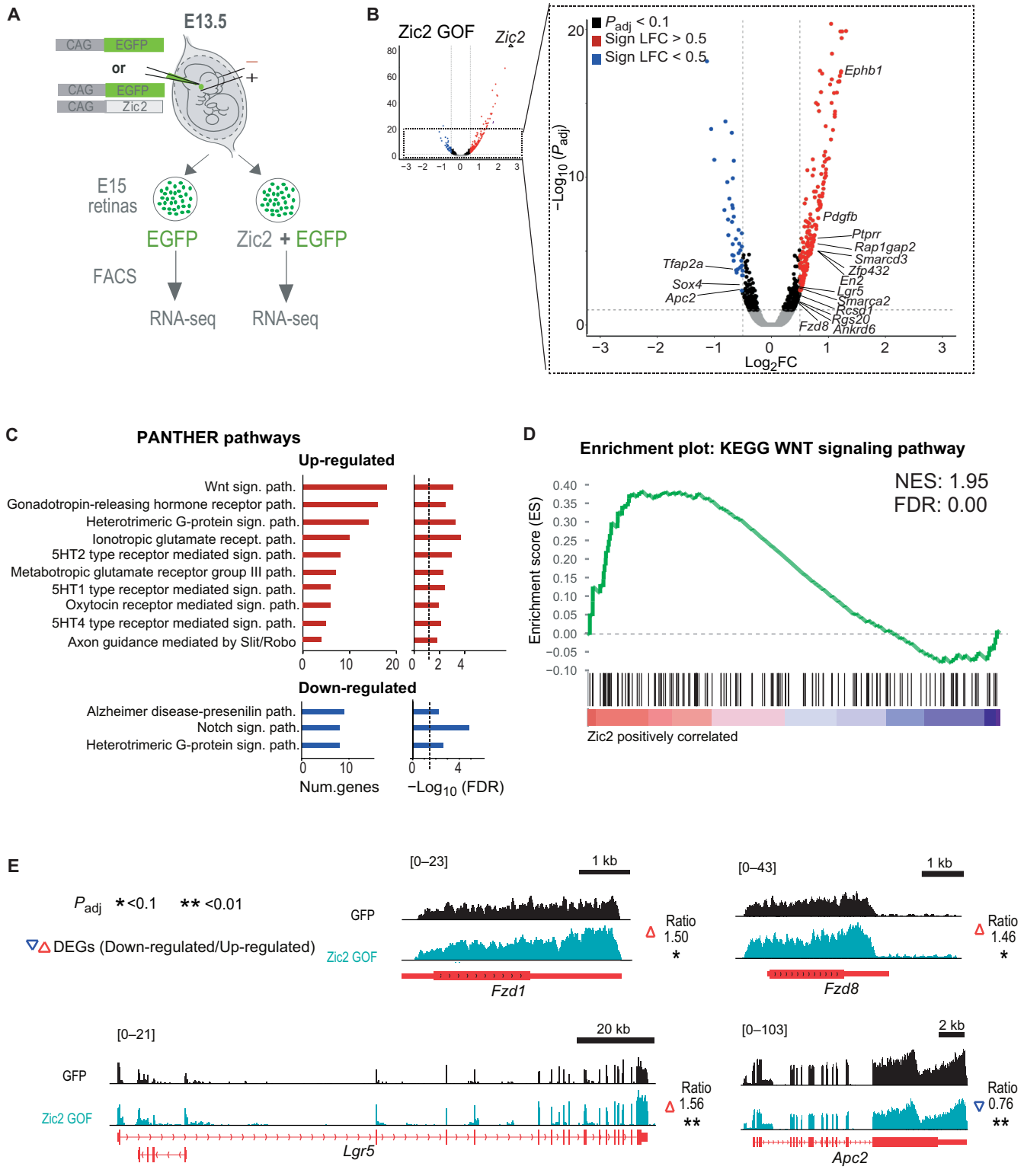

Fig. 4. Zic2 regulates many genes involved in the Wnt signaling pathway. (**A**) Scheme representing the experimental design of the RNA-seq screen. FACS, fluorescence-activated cell sorting. (**B**) Volcano plot showing differentially expressed genes (DEGs) 36 hours after Zic2 electroporation in contralateral RGCs. The name of relevant DEGs is indicated in the amplification inset. The significance value for the change in Zic2 is above the scale. LFC, log2 fold change. (**C**) PANTHER pathway enrichment analysis of genes up-regulated (top graphs) and down-regulated (bottom graphs) after Zic2-induced expression in RGCs. The bar graphs present the significance of the enrichment (right) and the number of genes involved (left). (**D**) GSEA of DEGs after Zic2 transduction of RGCs detects a nonrandom distribution of genes involved in Wnt signaling. The normalized enrichment score (NES) and false discovery rate (FDR) values are shown in the upper right corner of the graph. (**E**) Examples of RNA-seq profiles from relevant Wnt signaling genes down-regulated (*Apc2*) or up-regulated (*Fzd1*, *Fzd8*, and *Lgr5*) by Zic2.

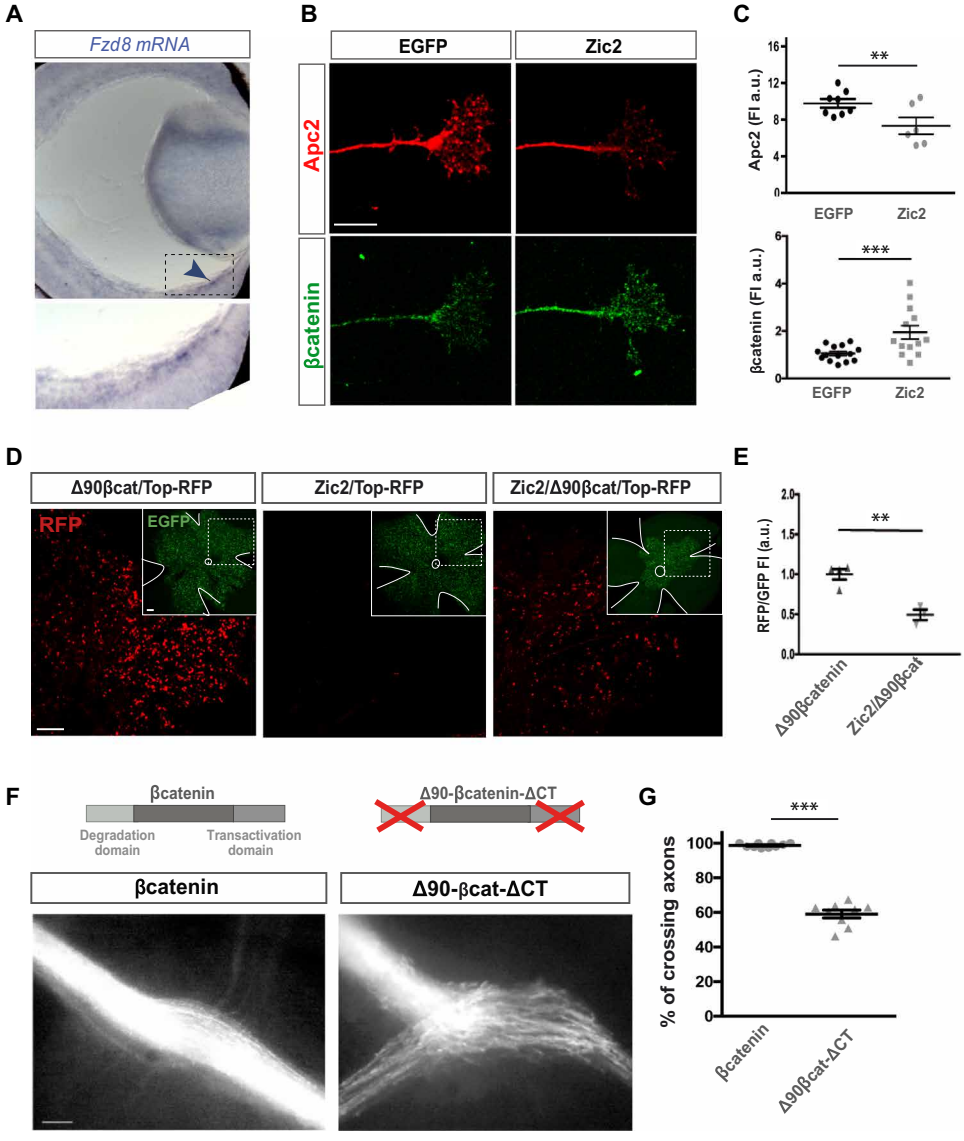

Fig. 5. Zic2 activates a program that leads to the accumulation of βcatenin in RGC axons. (**A**) In situ hybridization for Fzd8 in a coronal section of an E16.5 mouse retina. Bottom panel shows higher magnification of the squared area. (**B**) Immunofluorescence for Apc2 and βcatenin in the growth cone of axons growing from explants electroporated with EGFP- or Zic2-encoding plasmids. Scale bar, 10 μm. (**C**) Quantification of immunofluorescence intensity for Apc2 (upper graph) and βcatenin (lower graph) (**$P < 0.01$ and ***$P < 0.001$) (n = mean of at least four growth cones/explant). (**D**) RFP fluorescence in whole-mount E16.5 retinas electroporated at E13.5 with the indicated plasmids. Panels at the right corner show targeted/EGFP cells in the same whole-mounted retinas. Scale bar, 100 μm. (**E**) Normalized quantification of RFP fluorescence intensity in whole-mount electroporated retinas. n = number of retinas (unpaired t test with Welch's correction, **$P < 0.001$). (**F**) Optic chiasms from E16.5 embryos electroporated with plasmids encoding for βcatenin or Δ90-βCatenin-ΔCT. Scale bar, 100 μm. (**G**) Percentage of contralaterally projecting axons at the optic chiasm normalized to the total number of targeted axons (n = number of embryos) (two-tailed unpaired t test, ***$P < 0.001$). Results show means ± SEM. All results come from at least three independent experiments.

with axons choosing either the ipsilateral or the contralateral route (Fig. 5, F and G).

EphB1-mediated asymmetric phosphorylation of βcatenin may facilitate axon steering

Previous reports have shown that the tyrosine kinase receptor EphB1, a direct target for Zic2, is necessary for the ipsilateral projection to form (*18*). However, electroporation of EphB1 in RGCs was known to induce midline avoidance with much less efficiency than electroporation of Zic2 (*17*, *32*). This already pointed to the existence of mechanisms, additional to EphB/ephrinB signaling, involved in axon midline avoidance, but such mechanisms had remained unknown. Our βcatenin gain- and loss-of-function results suggested that alterations on the polarized accumulation of βcatenin are also involved in the decision of crossing or not the midline (Figs. 2 and 5). We hypothesized that abolishing the capacity of the axon to asymmetrically accumulate βcatenin, and inducing EphB1 at the same time, should increase the number of axons steering at the midline compared to simple induction of EphB1. To test this idea, we electroporated EphB1- and ctnnb1

shRNA–encoding plasmids at E13.5 and analyzed the optic chiasms of electroporated embryos 5 days later. As expected, blocking the capacity of the axons to respond to Wnt5a by reducing the levels of βcatenin and concomitantly inducing the expression of EphB1 almost doubled the number of axons changing their laterality compared to when only EphB1 plasmids were electroporated (Fig. 6, A to C).

These results suggested that ipsilateral neurons need to silence the positive response to Wnt5a to prevent crossing at the same time that inducing asymmetric cytoskeleton destabilization upon activation of EphB1 to promote steering. To date, there is no evidence showing interactions between βcatenin and Eph receptors, but crosstalk between these membrane proteins and Wnt signaling has been suggested in oncogenic contexts (*33*). It is known that βcatenin links membrane-integrated cadherins to actin filaments and promotes cytoskeleton stabilization (*34*–*36*), and the levels and subcellular localization of βcatenin as well as the interaction with cadherin are tightly regulated by phosphorylation (*37*). Taking all these observations into account, we considered the idea that EphB1 phosphorylates βcatenin to facilitate asymmetric cadherin–actin filament disassembly in ipsilaterally projecting neurons.

To tackle this hypothesis, we activated the EphB1 receptor by overexpression (*38*) in human embryonic kidney (HEK) 293 cells and performed immunoprecipitation assays using antibodies against βcatenin and phosphotyrosine. We also transfected HEK293 cells with an EGFP-encoding plasmid or with plasmids containing a truncated version of the EphB1 receptor lacking the kinase domain (EphB1-ΔCT) as a control. We detected a large enrichment of βcatenin in the pool of immunoprecipitated tyrosine-phosphorylated proteins obtained from EphB1-transfected cells compared to GFP- and EphB1-ΔCT–transfected cells (Fig. 6C). Consistently, we observed tyrosine phosphorylation at a band that corresponds to the molecular weight of βcatenin in immunoprecipitations by using an antibody against βcatenin. This phospho-Tyr band was much stronger in extracts from EphB1-transfected cells than from GFP- and EphB1-ΔCT–transfected cells (Fig. 6D). Both experiments indicate that βcatenin is phosphorylated at tyrosine residue/s by EphB1. Furthermore, mass spectrophotometry analysis of the immunoprecipitated product revealed that βcatenin phosphorylation occurs at the tyrosine residue 654 (Y654) upon EphB1 activation (Fig. 6E).

pY654-βcatenin has a reduced affinity for the cadherins integrated in the cell membrane (*34*). Consistent with this, we detected Y654-βcatenin by immunofluorescence at the cytoplasm rather than in the plasma membrane and totally excluded from the nuclei of cells transfected with EphB1 plasmids. In addition, Y654-βcatenin cells exhibited smaller areas and adopted rounded shapes compared to control cells that occupied an extended area and exhibited more polygonal silhouettes (Fig. 6, F to H), indicating an increase in cell detachment induced by EphB1-mediated phosphorylation of βcatenin at the Y654. In line with these results, we also detected an elevated number of cells positive for Y654-βcatenin in retinal explants electroporated with EphB1-encoding plasmids, demonstrating that EphB1-mediated βcatenin phosphorylation also occurs in retinal neurons (Fig. 6I). Together, these results support a model in which EphB1 asymmetrically phosphorylates βcatenin in the growth cone upon activation of ephrinB2 expressed at midline to prevent the formation of cadherin–actin filament complexes and facilitate axon steering.

DISCUSSION

A βcatenin-dependent but noncanonical Wnt pathway plays an essential role in axon guidance

The participation and the mode of action of the Wnt signaling pathways in axon guidance have been a controversial issue for years (*6*, *13*, *39*–*41*). Our results reconcile all the previous observations about the participation of the canonical versus the noncanonical Wnt pathway in axon navigation by revealing a third via that regulates crossing and it is independent on βcatenin-mediated transcription but relays on its local accumulation. This form of signal transduction is remarkably different to the canonical pathway because the changes in βcatenin stability are restricted to the axon terminal compartment and never reaches the cell nucleus or triggers transcription. However, because it involves βcatenin dynamics, it is not the classical PCP pathway either.

Our results support a model in which Wnt5a binding induces polarized accumulation of βcatenin in contralaterally projecting axons, likely activated by the expression of Fzd2, Fzd5, and/or Ryk (fig. S3F), which, in turn, leads to cytoskeleton stabilization at the tip of the growth cone and promotes midline crossing. In contrast, the presence of the TF Zic2 in ipsilaterally projecting neurons induces a gene program that silences this positive response to Wnt5a and triggers instead a different set of Wnt receptors that, together with the EphB1-dependent phosphorylation of βcatenin, allows membrane detachment by disrupting the binding of membrane-associated cadherins with actin filaments (Fig. 7).

It has been suggested that ipsilateral axons are repelled by contralateral axons in a Sonic Hedgehog–mediated manner (*42*). We cannot discard a similar scenario in the response of iRGC axons to Wnt5a. However, given the intrinsic regulation of Wnt-related proteins by Zic2, we favor the idea that the negative response of iRGC axons to Wnt5a is direct rather than through cRGCs.

Together, our findings clarify many aspects of the long-standing debate about Wnt signaling pathways in axon pathfinding. First, this work shows that Wnt5a elicits attractive or repulsive responses in the same type of neurons depending on a particular transcriptional program that controls the expression of a set of Wnt receptors and Wnt-related intracellular proteins. Second, they reveal that axon repulsion cannot be achieved only through the action of repulsive receptors since ipsilateral axons need to silence attractive mechanisms for effective steering. Last, they also clarify that Wnts do not activate the canonical or PCP pathways in axon guidance processes, but much more complex mechanisms based on βcatenin dynamics at the growth cone mediate axonal navigation.

Zic2 regulation of the Wnt pathway likely operates in many contexts

Our study not only reveals a previously unknown branch of the Wnt signaling pathway but also identifies the TF responsible for a two-way switch in the transduction on this previously unidentified Wnt pathway. We propose that a similar switch in the response to Wnt ligands may operate in other tissues and contexts where Wnt signaling and Zic2 coexist beyond axon guidance. For instance, Zic proteins are expressed in several populations of migrating neuroblasts in the forebrain, hindbrain, and neural tube as well as in neural stem cells in the adult individual (*43*–*48*). In all these contexts, cells expressing Zic TFs are in contact with Wnt proteins (*43*) and delaminate from a neuroepithelium undergoing shape rearrangements before migrating through stereotyped paths. Ipsilaterally projecting neurons, or

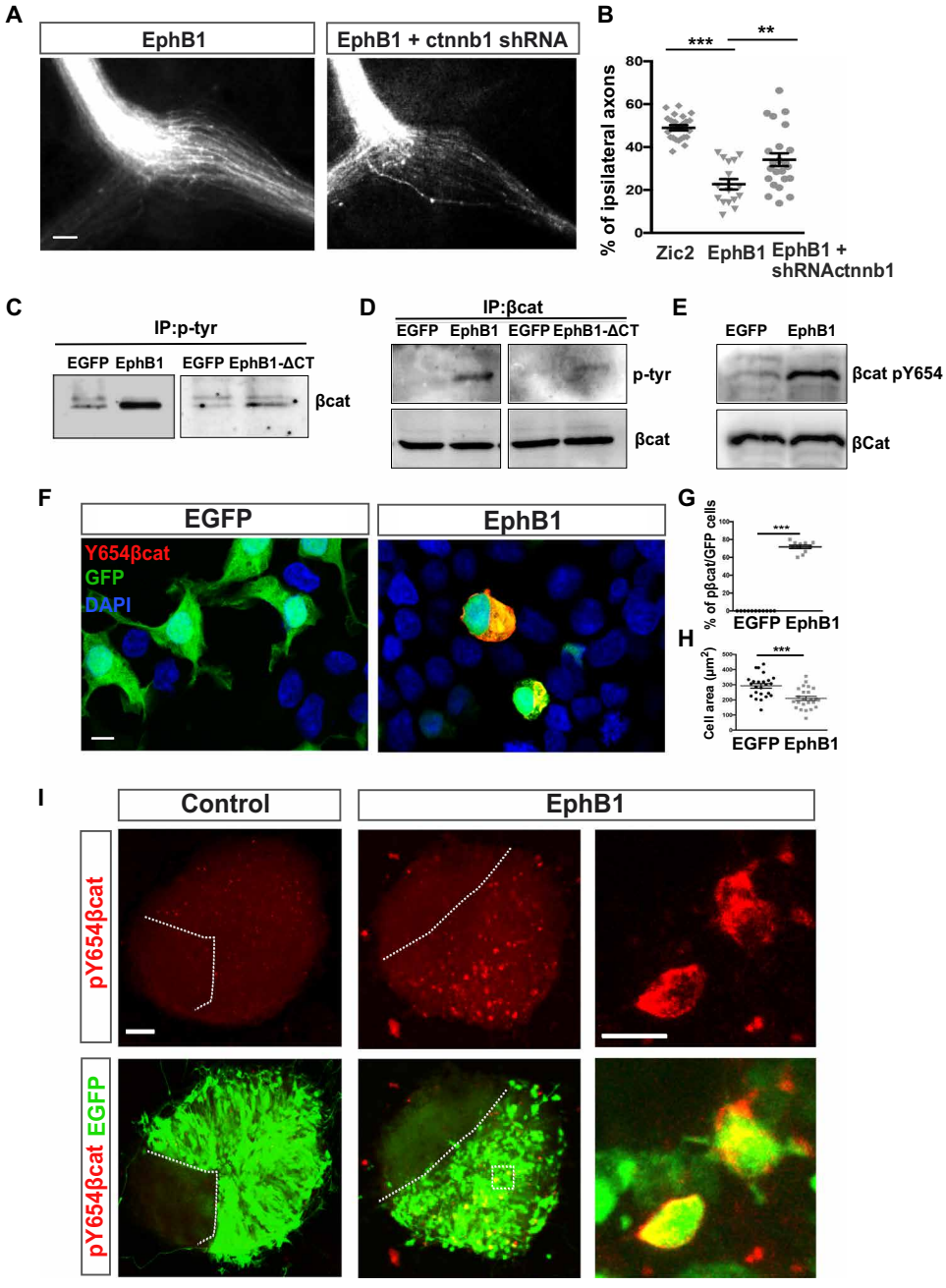

Fig. 6. EphB1 phosphorylates βcatenin. (**A**) Optic chiasms from E16.5 embryos electroporated at E13.5 with plasmids encoding EGFP plus EphB1 alone or together with plasmids bearing shRNA against βcatenin (ctnnb1 shRNA). Scale bar, 100 μm. (**B**) Quantification showing the percentage of ipsilaterally projecting axons in each condition normalized to the total number of EGFP axons at the chiasm (*n* = number of embryos) (two-tailed unpaired *t* test, $^{**}P < 0.01$ and $^{***}P < 0.001$). Results show means ± SEM. (**C**) Detection of βcatenin in the immunoprecipitation (IP) of tyrosine-phosphorylated proteins from GFP-, EphB1-, and EphB1-ΔCT–transfected cells. (**D**) Detection of tyrosine phosphorylation in βcatenin immunoprecipitated from GFP-, EphB1-, and EphB1-ΔCT–transfected cells. (**E**) Detection of Y654-βcatenin in protein extracts from GFP- and EphB1-transfected cells. (**F**) Immunohistochemistry using antibodies to Y654-βcatenin and total βcatenin in HEK293 cells transfected with EGFP or EphB1. Scale bar, 10 μm. DAPI, 4′,6-diamidino-2-phenylindole. (**G**) Percentage of phospho–Y654-βcatenin cells on EGFP-expressing cells. Eleven regions of interest (ROIs) were quantified from three independent experiments for each condition. Two-tailed Mann-Whitney test ($^{***}P < 0.001$). Results show means ± SEM. (**H**) Quantification of the area occupied by individual cells transfected with EGFP alone or EphB1- and EGFP-encoding plasmids (*n* = number of cells). Two-tailed unpaired *t* test ($^{***}P < 0.001$). Results show means ± SEM. (**I**) pY654βcatenin immunostaining in retinal explants electroporated with EGFP- or EphB1/EGFP-encoding plasmids. Scale bar, 50 μm. Scale bar in the higher magnification panels at the right, 10 μm. Representative experiments from three independent experiments are shown.

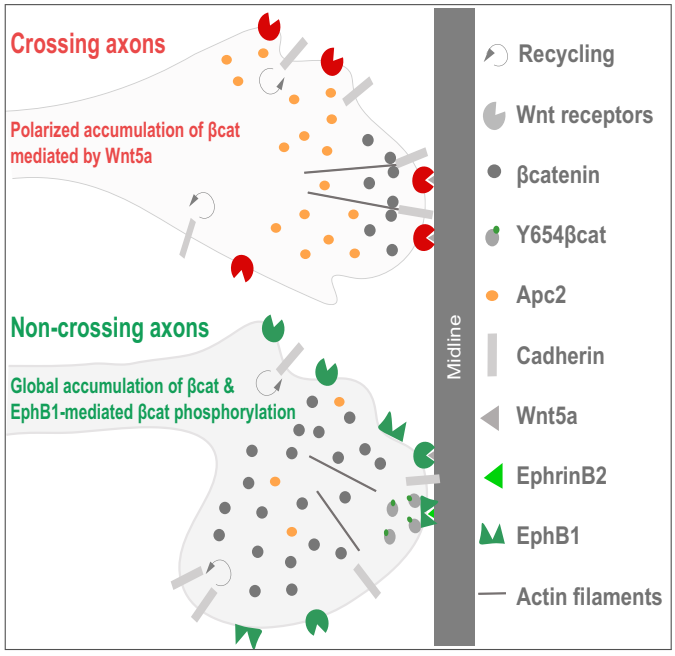

Fig. 7. Working model. It has been widely demonstrated that when the axon grows in the absence of Wnt5a, cadherins are constantly being recycled from the plasma membrane. Our results support a model in which midline-expressed Wnt5a triggers local accumulation of βcatenin in contralateral axons. It has been shown that βcatenin links cadherins and actin microtubules. Thus, Wnt5a-dependent accumulation of βcatenin would facilitate midline crossing by promoting the stabilization of the cytoskeleton at the tip of the growth cone. In contrast, our results demonstrate that Zic2 activates a different set of Wnt receptors and other intracellular Wnt proteins in ipsilaterally projecting neurons, such as Fzd1, Fzd8, Lgr5, or Apc2, to favor the accumulation of βcatenin. We also show that EphB1 phosphorylates βcatenin in Y654, and previous reports have demonstrated that phosphorylated Y654-βcatenin has low affinity for cadherins. Taking all these observations together, we propose that phosphorylation of βcatenin induced by the binding of EphB1 to ephrinB2 prevents the formation of cadherin/actin complexes facilitating axon steering.

at least an important number of them, also originate from an epithelium-like area known as the ciliary marginal zone (*20*, *49*), and the cell bodies of these cells are exposed to Wnt ligands secreted from this peripheral retinal area (*50*, *51*). In these cells, Zic2 likely plays a twofold function regarding Wnt signaling. In addition, to regulate axon guidance as we show here, it would block the canonical pathway to prevent proliferation, guaranteeing that the recently differentiated neurons do not reenter the cell cycle. Consistent with this idea, it has been shown that activation of Wnt signaling alters the number of ipsilaterally projecting neurons potentially by keeping them in the cell cycle (*19*). Furthermore, experiments in zebrafish and human cell lines suggest that Zic2 blocks the canonical Wnt signaling pathway (*52*), a result that we have also confirmed here and that could occur in particular contexts concomitantly with its role in regulating the alternative βcatenin-dependent but noncanonical Wnt pathway.

Zic2 mutations in mice and humans cause holoprosencephaly type IV, anencephaly, and spina bifida (*53*, *54*) likely as a consequence of defects in early developmental stages such as gastrulation and/or neurulation (*45*, *55*). In addition, accumulating evidence shows that this TF is up-regulated in many different types of cancer (*56*). However, the molecular mechanisms underlying these Zic2-associated anomalies have remained largely elusive. Wnt and Eph/ephrin pathways both play key functions in all these processes. While further experiments should revisit the role of Zic2 in early development and oncogenic scenarios, our results support the idea that Zic2 may regulate the cross-talk between the Eph and Wnt pathways in many different contexts.

MATERIALS AND METHODS

Mice

B6.FVB(Cg)-Tg(Slc6a4-cre)ET33Gsat (stock number, MMRC 031028-UCD) mice were crossed with the reporter line B6.Cg-*Gt(ROSA)26Sor*$^{tm14(CAG-tdTomato)Hze}$ (The Jackson Laboratory, stock number 007914) to obtain Sert-RFP embryos. All the electroporation experiments were performed using embryos from C57/DBA F1 hybrids. Mice were kept in a timed pregnancy breeding colony at the Instituto de Neurociencias (IN). The animal protocols were approved by the IN Animal Care and Use Committee and met European and Spanish regulations.

In utero electroporation and quantification

Time-pregnant female mice were anesthetized with a classic small-animal anesthesia (isoflurane) system (WPI, USA). In utero electroporation was performed as described in (*57*). Plasmids with pCAG-hZic2 (*58*), pCAG-Δ90-βCatenin-GFP (Addgene 26645), pCAG-FullβCatenin-GFP, pCAG-Δ90-βCatenin-ΔCT-GFP, pCAG-EphB1, and Top-RFP were injected at 1 μg/μl and pSilencer-sh-ctnnb1 and pSilencer-control at 2 μg/μl. pCAG-GFP plasmids were co-injected at 0.5 μg/μl. pCAG-Δ90-βCatenin-ΔCT-GFP and pCAG-FullβCatenin-GFP were obtained from manipulation of the CAG-Δ90-βCatenin-GFP. Fiji software was used to quantify contralateral and ipsilateral projections. Briefly, mean fluorescence intensity from three linear regions of interest (ROIs) drawn perpendicularly on each optic tract (OTF) was measured, and background from a very proximal area was rested to each measure. The percent of ipsilateral projection was determined for each individual embryo by applying the following formula: % Ipsis = (iOTF × 100)/(iOTF + cOTF). Statistical analyses were performed with GraphPad Prism 6.0 (GraphPad Software Inc., La Jolla, CA).

Retinal explant cultures and immunohistochemistry

Retinal explants from E14.5/E15.5 WT or electroporated embryos were plated on glass-bottom microwell dishes (MatTek) coated with poly-L-lysine (0.01%) and laminin (20 μg/ml). Culture medium was Dulbecco's modified Eagle's medium (DMEM):F12/neurobasal medium (Gibco) with 0.4% of methylcellulose with growth supplements N-2 and B-27 and antibiotics penicillin/streptomycin. For axonal growth analysis, recombinant Wnt5a (recombinant human/mouse Wnt5a, R&D Systems, reference 645-WN) at 200 ng/ml or Wnt5a reconstitution buffer as a vehicle was added to the medium. For acute responses, retinal explants were exposed to recombinant Wnt5a at 200 ng/ml for 1 hour.

Immunohistochemistry was performed on retinal explants fixed with prewarmed 4% paraformaldehyde (PFA) in phosphate-buffered saline (PBS) at 37°C for 20 min. Explants were permeabilized with 0.025% Triton X-100, blocked with horse serum, and incubated with the specified antibody at 4°C overnight. The following antibodies were used: chicken anti-GFP (Aves Labs, GFP-1020), rabbit anti-RFP (Rockland, 600-401-379), mouse anti-βcatenin (BD Transduction

Laboratories, 610153), rabbit anti-APC2 (Fisher, PA5-20944), rabbit anti-pY654-βcatenin (Abcam, Ab59430), and Alexa Fluor 488 phalloidin (Invitrogen, A12379). Fluorescence microscopy was performed using a Leica SPEII confocal microscope. Area and fluorescence intensities at the growth cones were normalized using phalloidin staining and quantified by Fiji software using maximum intensity *z* projection. RFP or GFP growth cones with areas of <70 μm were considered as collapsed, and the percent of collapsed axons was referred to the total number of RFP- or GFP-positive axons in the explant.

In situ hybridization

Heads of embryos from E13.5 to E17.5 were dissected in 1× cold PBS and fixed in 4% PFA overnight. Coronal vibrosections (optic chiasms) or cryosections (retinas) were obtained, and in situ hybridization with specific antisense riboprobes generated from complementary DNAs (cDNAs) for Fzd8 [NM_008058.2; 65 to 870 base pairs (bp); gift of P. Bovolenta, Centro de Biología Molecular Severo Ochoa (CBMSO), Spain], Wnt1 (NM_021279.4; 1100 to 2118 bp; gift of S. Martinez, Instituto de Neurociencias de Alicante, Spain), Wnt5a (NM_009524.4; 1143 to 2166 bp), and Wnt11 (NM_ 001285792.1; 589 to 1644 bp; both gifts of E. David, University of Rochester, NY, USA) was performed. Images were captured with Leica DM2500 equipped with a Leica DFC7000 T camera and Leica Application Suite version 4.10.0 software.

RNA-seq and bioinformatic analyses

RGCs from E13 electroporated retinas were isolated 36 hours after electroporation by cell sorting. Isolated retinas were enzymatically dissociated in a mixture of collagenase/trypsin and bovine serum albumin for 20 min at 37°C followed by mechanical dissociation. Single-cell suspension was filtered and resuspended in cold Hanks' balanced salt solution medium supplemented with 20% fetal bovine serum (FBS). After cell sorting, cells were centrifuged and frozen. Total RNA extraction was performed with the Arcturus PicoPure RNA Isolation Kit (Thermo Fisher Scientific). The samples were sequenced according to the manufacturer's instructions in HiSeq Sequencing v4 Chemistry (Illumina Inc.). Briefly, RNA-seq reads were mapped to the mouse genome (Mus_musculus.GRCm.38.83) using STAR (v2.5.0c) (*59*). Quality control of the raw data was performed with FastQC (www.bioinformatics.babraham.ac.uk/projects/fastqc/). Library sizes were between 41 and 75 million single reads. Samtools (v1.3.1) was used to handle BAM files (*60*). To retrieve differentially expressed genes (DEGs), mapped reads were counted with HTSeq v0.6.1 (*61*) with the following parameters: -s reverse, –i gene_id, and with a gtf file reference of GRCm38.83. Read count tables were analyzed using DESeq2 v1.10.0 (*62*). Analysis and preprocessing of data were performed with custom scripts using R (https://cran.r-project.org/) (v3.4.3 "Kite-Eating Tree") statistical computing and graphics and Bioconductor v3.2 (BiocInstaller 1.20.3) (*63*). Genes were considered differentially expressed at Benjamini-Hochberg–adjusted *P* value < 0.1. Significantly up-regulated and down-regulated genes were visualized with Integrative Genomics Viewer (IGV) (v2.3.72) (*64*). Gene Ontology (GO) enrichment analyses were performed using the platform PANTHER (*65*), with Fisher's exact test and with the P_{adj} correction, obtaining the top terms using the filters by ratio enrichment of >2, number of GO family group genes between 3 and 2000, number of enrichment genes of >3, and P_{adj} of <0.1. The gene set enrichment analysis was obtained with GSEA v3.0 (*66*).

Sample	Library type	No. of reads	Type of sequencing	Read length
GFP1	RNA-seq	43381301	Single end	50
GFP2	RNA-seq	41842837	Single end	50
GFP3	RNA-seq	46718303	Single end	50
Zic2.1	RNA-seq	45279883	Single end	50
Zic2.2	RNA-seq	34371605	Single end	50
Zic2.3	RNA-seq	76525940	Single end	50

Datasets can be accessed at the Gene Expression Omnibus (GEO) repository (GSE133492).

Immunoprecipitation, Western blot, and mass spectrometry

HEK293 [American Type Culture Collection (ATCC) CRL-15736] cultured according to standard conditions were transfected with pCAG-FullβCatenin-GFP or pCAG-FullβCatenin-GFP/pCAG-EphB1 and isolated by cell sorting 48 hours after transfection. Total protein was extracted in radioimmunoprecipitation assay (RIPA) buffer with protease and phosphatase inhibitors. Immunoprecipitation and Western blot analysis were performed on total protein samples from HEK293 cells 24 hours after transfection with EGFP-EphB1 or EphB1-ΔCT–bearing plasmids in RIPA buffer supplemented with protease and phosphatase inhibitors. For immunoprecipitations, antibodies were used at 1:500 and precipitated with protein G Sepharose beads. To validate the sh-ctnnb1–bearing plasmids, N2a cells (ATCC CCL-131) cultured according to standard conditions in 24-well plates were transfected with sh-ctnnb1 or random shRNAs at 0.5 and 1 μg per well. pCAG-GFP plasmid was cotransfected to assay transfection efficiency. All samples were resolved by SDS–polyacrylamide gel electrophoresis. Rabbit anti-GAPDH (glyceraldehyde-3-phosphate dehydrogenase) (G9545), anti-mouse HRP (horseradish peroxidase) (Sigma-Aldrich, A4416), and anti-rabbit HRP (Sigma-Aldrich, A9169) were used for Western blot. The rest of the antibodies used in the Western blot are the same as those used in immunohistochemistry. To obtain a phosphotyrosine-enriched βcatenin sample for the mass spectrometry analysis, a tandem enrichment strategy was used. First, immunoprecipitation was performed with an anti-phosphotyrosine antibody (Millipore, 05-321), and protein G–bounded proteins were eluted with phenyl phosphate (100 mM) and then immunoprecipitated with anti-βcatenin antibody (BD Transduction Laboratories, 610153). Samples were analyzed by mass spectrometry. Protein identification by liquid chromatography–tandem mass spectrometry (LC-MS/MS) (LTQ Orbitrap Velos) was carried out in the CBMSO Protein Chemistry Facility, which belongs to ProteoRed, PRB2-ISCIII, supported by grant PT13/0001. Immunoprecipitation and Western blot analysis were performed on total protein samples from HEK293 cells 24 hours after transfection with EGFP-, EphB1-, or EphB1-ΔCT–bearing plasmids in RIPA buffer supplemented with protease and phosphatase inhibitors. For immunoprecipitations, antibodies were used at 1:500 and precipitated with protein G Sepharose beads.

Data collection and analysis

Data collection was performed using the following equipment: FACSAria2, Illumina NovaSeq, Leica SPEII confocal microscope, Leica DM2500, Leica DFC7000 T camera, and CUY21SC electroporator. Data analysis was performed using the following software: FlowJo

v10, Fiji software maximum intensity *z* projection, Leica Application Suite software, ImageJ (v2), Microsoft Excel (v16), FastQC (v.0.11.6), RSeQC (v2.6.4), fastq-dump (v2.3.5), Python 3.7.3, R software (v3.4.4), Cutadapt (v1.18), Samtools (v1.9), Bedtools (v2.26.0), Rsubread (v1.26.0), STAR (v2.5.0a), HTSeq (v0.7.2), DESeq2 (v1.10.0), GSEA (v4.0.3), biomaRt (v2.39), PANTHER (v14), IGV (v2.3.92), HOMER (v4.8), MEME Suite (v5.0.3), and GraphPad Prism software (v7.0), San Diego. Statistical analysis was performed as indicated in figure legends. Sample size was estimated according to data variance and correlation between biological replicates and distance to control condition. Each analysis was done in accordance to the sample size, sequencing depth, and conditions. Reproducibility across replicate was very high. The measures applied to evaluate replicates were correlation among samples, variance, Euclidean classification, principal components analysis, and statistical tests that revealed no significant differences within the group. In the analyses in which a replicate was not available, analyses were supported by the use of internal controls and the sample was normalized and compared with samples from related conditions in which replicates were available [i.e., analysis of variance (ANOVA) and DESeq2].

SUPPLEMENTARY MATERIALS

Supplementary material for this article is available at http://advances.sciencemag.org/cgi/content/full/6/46/eaaz8797/DC1

View/request a protocol for this paper from *Bio-protocol*.

REFERENCES AND NOTES

1. A. Chédotal, Roles of axon guidance molecules in neuronal wiring in the developing spinal cord. *Nat. Rev. Neurosci.* **20**, 380–396 (2019).
2. E. T. Stoeckli, Understanding axon guidance: Are we nearly there yet? *Development* **145**, dev151415 (2018).
3. E. Herrera, L. Erskine, C. Morenilla-Palao, Guidance of retinal axons in mammals. *Semin. Cell Dev. Biol.* **85**, 48–59 (2019).
4. L. G. Fradkin, J. N. Noordermeer, R. Nusse, The Drosophila Wnt protein DWnt-3 is a secreted glycoprotein localized on the axon tracts of the embryonic CNS. *Dev. Biol.* **168**, 202–213 (1995).
5. S. Yoshikawa, R. D. McKinnon, M. Kokel, J. B. Thomas, Wnt-mediated axon guidance via the Drosophila derailed receptor. *Nature* **422**, 583–588 (2003).
6. A. I. Lyuksyutova, C.-C. Lu, N. Milanesio, L. A. King, N. Guo, Y. Wang, J. Nathans, M. Tessier-Lavigne, Y. Zou, Anterior-posterior guidance of commissural axons by Wnt-frizzled signaling. *Science* **302**, 1984–1988 (2003).
7. C. Jamora, E. Fuchs, Intercellular adhesion, signalling and the cytoskeleton. *Nat. Cell Biol.* **4**, E101–E108 (2002).
8. T. P. Rao, M. Kühl, An updated overview on Wnt signaling pathways: A prelude for more. *Circ. Res.* **106**, 1798–1806 (2010).
9. A. G. Fenstermaker, A. A. Prasad, A. Bechara, Y. Adolfs, F. Tissir, A. Goffinet, Y. Zou, R. J. Pasterkamp, Wnt/planar cell polarity signaling controls the anterior-posterior organization of monoaminergic axons in the brainstem. *J. Neurosci.* **30**, 16053–16064 (2010).
10. B. Shafer, K. Onishi, C. Lo, G. Colakoglu, Y. Zou, Vangl2 promotes Wnt/planar cell polarity-like signaling by antagonizing Dvl1-mediated feedback inhibition in growth cone guidance. *Dev. Cell* **20**, 177–191 (2011).
11. F. Tissir, I. Bar, Y. Jossin, O. De Backer, A. M. Goffinet, Protocadherin Celsr3 is crucial in axonal tract development. *Nat. Neurosci.* **8**, 451–457 (2005).
12. G. Chai, L. Zhou, M. Manto, F. Helmbacher, F. Clotman, A. M. Goffinet, F. Tissir, Celsr3 is required in motor neurons to steer their axons in the hindlimb. *Nat. Neurosci.* **17**, 1171–1179 (2014).
13. E. C. Avilés, E. T. Stoeckli, Canonical wnt signaling is required for commissural axon guidance. *Dev. Neurobiol.* **76**, 190–208 (2016).
14. A. J. Mikels, R. Nusse, Purified Wnt5a protein activates or inhibits β-catenin–TCF signaling depending on receptor context. *PLOS Biol.* **4**, e115 (2006).
15. E. Herrera, L. Brown, J. Aruga, R. A. Rachel, G. Dolen, K. Mikoshiba, S. Brown, C. A. Mason, Zic2 patterns binocular vision by specifying the uncrossed retinal projection. *Cell* **114**, 545–557 (2003).
16. A. Escalante, B. Murillo, C. Morenilla-Palao, A. Klar, E. Herrera, Zic2-dependent axon midline avoidance controls the formation of major ipsilateral tracts in the CNS. *Neuron* **80**, 1392–1406 (2013).
17. C. García-Frigola, M. I. Carreres, C. Vegar, C. Mason, E. Herrera, Zic2 promotes axonal divergence at the optic chiasm midline by EphB1-dependent and -independent mechanisms. *Development* **135**, 1833–1841 (2008).
18. S. E. Williams, F. Mann, L. Erskine, T. Sakurai, S. Wei, D. J. Rossi, N. W. Gale, C. E. Holt, C. A. Mason, M. Henkemeyer, Ephrin-B2 and EphB1 mediate retinal axon divergence at the optic chiasm. *Neuron* **39**, 919–935 (2003).
19. L. Iwai-Takekoshi, R. Balasubramanian, A. Sitko, R. Khan, S. Weinreb, K. Robinson, C. Mason, Activation of Wnt signaling reduces ipsilaterally projecting retinal ganglion cells in pigmented retina. *Development* **145**, dev163212 (2018).
20. M. Fernández-nogales, V. Murcia-belmonte, H. Yu, E. Herrera, I. D. N. Csic-umh, C. Superior, D. I. C. Miguel, C. S. Juan, A. Ramón, Progress in retinal and eye research the peripheral eye: A neurogenic area with potential to treat retinal pathologies ? *Prog. Retin. Eye Res.* **68**, 110–123 (2019).
21. P. D. Mccrea, C. W. Turck, B. Gumbiner, A homolog of the armadillo protein in Drosophila (plakoglobin) associated with E-cadherin. *Science* **254**, 1359–1361 (1991).
22. M. A. Rabadán, A. Herrera, L. Fanlo, S. Usieto, C. Carmona-Fontaine, E. H. Barriga, R. Mayor, S. Pons, E. Martí, Delamination of neural crest cells requires transient and reversible Wnt inhibition mediated by Dact1/2. *Development* **143**, 2194–2205 (2016).
23. C. N. Wrobel, C. A. Mutch, S. Swaminathan, M. M. Taketo, A. Chenn, Persistent expression of stabilized β-catenin delays maturation of radial glial cells into intermediate progenitors. *Dev. Biol.* **309**, 285–297 (2007).
24. C. García-Frigola, E. Herrera, Zic2 regulates the expression of Sert to modulate eye-specific refinement at the visual targets. *EMBO J.* **29**, 3170–3183 (2010).
25. S. M. Koch, C. G. Dela Cruz, T. S. Hnasko, R. H. Edwards, A. D. Huberman, E. M. Ullian, Pathway-specific genetic attenuation of glutamate release alters select features of competition-based visual circuit refinement. *Neuron* **71**, 235–242 (2011).
26. T. Kuwajima, C. A. Soares, A. A. Sitko, V. Lefebvre, C. Mason, SoxC transcription factors promote contralateral retinal ganglion cell differentiation and axon guidance in the mouse visual system. *Neuron* **93**, 1110–1125.e5 (2017).
27. L. A. Quina, W. Pak, J. Lanier, P. Banwait, K. Gratwick, Y. Liu, T. Velasquez, D. D. M. O'Leary, M. Goulding, E. E. Turner, Brn3a-expressing retinal ganglion cells project specifically to thalamocortical and collicular visual pathways. *J. Neurosci.* **25**, 11595–11604 (2005).
28. W. Pak, R. Hindges, Y.-S. Lim, S. L. Pfaff, D. D. M. O'Leary, Magnitude of binocular vision controlled by Islet-2 repression of a genetic program that specifies laterality of retinal axon pathfinding. *Cell* **119**, 567–578 (2004).
29. E. Arbeille, G. J. Bashaw, Brain tumor promotes axon growth across the midline through interactions with the microtubule stabilizing protein Apc2. *PLOS Genet.* **14**, e1007314 (2018).
30. S. A. Purro, L. Ciani, M. Hoyos-Flight, E. Stamatakou, E. Siomou, P. C. Salinas, Wnt regulates axon behavior through changes in microtubule growth directionality: A new role for adenomatous polyposis coli. *J. Neurosci.* **28**, 8644–8654 (2008).
31. X. Lin, X. Liu, C. Gong, Expression of engrailed homeobox 2 regulates the proliferation, migration and invasion of non-small cell lung cancer cells. *Oncol. Lett.* **16**, 536–542 (2018).
32. T. J. Petros, B. R. Shrestha, C. Mason, Specificity and sufficiency of EphB1 in driving the ipsilateral retinal projection. *J. Neurosci.* **29**, 3463–3474 (2009).
33. H. Clevers, E. Batlle, EphB/EphrinB receptors and Wnt signaling in colorectal cancer: Figure 1. *Cancer Res.* **66**, 2–5 (2006).
34. K. Kim, K.-Y. Lee, Tyrosine phosphorylation translocates β-catenin from cell–cell interface to the cytoplasm, but does not significantly enhance the lef-1-dependent transactivating function. *Cell Biol. Int.* **25**, 421–427 (2001).
35. S. Roura, S. Miravet, J. Piedra, A. García de Herreros, M. Duñach, Regulation of E-cadherin/catenin association by tyrosine phosphorylation. *J. Biol. Chem.* **274**, 36734–36740 (1999).
36. J. Piedra, D. Martinez, J. Castano, S. Miravet, M. Dunach, A. G. de Herreros, Regulation of beta-catenin structure and activity by tyrosine phosphorylation. *J. Biol. Chem.* **276**, 20436–20443 (2001).
37. T. Valenta, G. Hausmann, K. Basler, The many faces and functions of β-catenin. *EMBO J.* **31**, 2714–2736 (2012).
38. S. H. Wimmer-Kleikamp, P. W. Janes, A. Squire, P. I. H. Bastiaens, M. Lackmann, Recruitment of Eph receptors into signaling clusters does not require ephrin contact. *J. Cell Biol.* **164**, 661–666 (2004).
39. A. M. Wolf, A. I. Lyuksyutova, A. G. Fenstermaker, B. Shafer, C. G. Lo, Y. Zou, Phosphatidylinositol-3-kinase-atypical protein kinase C signaling is required for Wnt attraction and anterior-posterior axon guidance. *J. Neurosci.* **28**, 3456–3467 (2008).
40. E. Domanitskaya, A. Wacker, O. Mauti, T. Baeriswyl, P. Esteve, P. Bovolenta, E. T. Stoeckli, Sonic hedgehog guides post-crossing commissural axons both directly and indirectly by regulating Wnt activity. *J. Neurosci.* **30**, 11167–11176 (2010).
41. P. Bovolenta, J. Rodriguez, P. Esteve, Frizzled/RYK mediated signalling in axon guidance. *Development* **133**, 4399–4408 (2006).
42. J. Peng, P. J. Fabre, T. Dolique, S. M. Swikert, L. Kermasson, T. Shimogori, F. Charron, Sonic hedgehog is a remotely produced cue that controls axon guidance trans-axonally at a midline choice point. *Neuron* **97**, 326–340.e4 (2018).

43. E. Herrera, Rodent Zic Genes in Neural Network Wiring. *Adv. Exp. Med. Biol.* **1046**, 209–230 (2018).
44. T. Inoue, M. Ota, K. Mikoshiba, J. Aruga, Zic2 and Zic3 synergistically control neurulation and segmentation of paraxial mesoderm in mouse embryo. *Dev. Biol.* **306**, 669–684 (2007).
45. J. J. TeSlaa, A. N. Keller, M. K. Nyholm, Y. Grinblat, Zebrafish Zic2a and Zic2b regulate neural crest and craniofacial development. *Dev. Biol.* **380**, 73–86 (2013).
46. B. Murillo, N. Ruiz-Reig, M. Herrera, A. Fairén, E. Herrera, Zic2 controls the migration of specific neuronal populations in the developing forebrain. *J. Neurosci.* **35**, 11266–11280 (2015).
47. F. T. Merkle, L. C. Fuentealba, T. A. Sanders, L. Magno, N. Kessaris, A. Alvarez-Buylla, Adult neural stem cells in distinct microdomains generate previously unknown interneuron types. *Nat. Neurosci.* **17**, 207–214 (2014).
48. M.-C. Tiveron, C. Beclin, S. Murgan, S. Wild, A. Angelova, J. Marc, N. Coré, A. de Chevigny, E. Herrera, A. Bosio, V. Bertrand, H. Cremer, Zic-proteins are repressors of dopaminergic forebrain fate in mice and C. Elegans. *J. Neurosci.* **37**, 10611–10623 (2017).
49. F. Marcucci, V. Murcia-Belmonte, Q. Wang, Y. Coca, S. Ferreiro-Galve, T. Kuwajima, S. Khalid, M. E. Ross, C. Mason, E. Herrera, The ciliary margin zone of the mammalian retina generates retinal ganglion cells. *Cell Rep.* **17**, 3153–3164 (2016).
50. T. Denayer, M. Locker, C. Borday, T. Deroo, S. Janssens, A. Hecht, F. van Roy, M. Perron, K. Vleminckx, Canonical Wnt signaling controls proliferation of retinal stem/progenitor cells in postembryonic *Xenopus* eyes. *Stem Cells* **26**, 2063–2074 (2008).
51. J. R. Meyers, L. Hu, A. Moses, K. Kaboli, A. Papandrea, P. A. Raymond, β-catenin/Wnt signaling controls progenitor fate in the developing and regenerating zebrafish retina. *Neural Dev.* **7**, 30 (2012).
52. R. Pourebrahim, R. Houtmeyers, S. Ghogomu, S. Janssens, A. Thelie, H. T. Tran, T. Langenberg, K. Vleminckx, E. Bellefroid, J.-J. Cassiman, S. Tejpar, Transcription factor Zic2 inhibits Wnt/β-catenin protein signaling. *J. Biol. Chem.* **286**, 37732–37740 (2011).
53. S. A. Brown, D. Warburton, L. Y. Brown, C.-y. Yu, E. R. Roeder, S. Stengel-Rutkowski, R. C. M. Hennekam, M. Muenke, Holoprosencephaly due to mutations in ZIC2, a homologue of Drosophila odd-paired. *Nat. Genet.* **20**, 180–183 (1998).
54. T. Nagai, J. Aruga, O. Minowa, T. Sugimoto, Y. Ohno, T. Noda, K. Mikoshiba, Zic2 regulates the kinetics of neurulation. *Proc. Natl. Acad. Sci. U.S.A.* **97**, 1618–1623 (2000).
55. R. Houtmeyers, O. Tchouate Gainkam, H. A. Glanville-Jones, B. Van den Bosch, A. Chappell, K. S. Barratt, J. Souopgui, S. Tejpar, R. M. Arkell, *Zic2* mutation causes holoprosencephaly via disruption of NODAL signalling. *Hum. Mol. Genet.* **25**, 3946–3959 (2016).
56. R. Houtmeyers, J. Souopgui, S. Tejpar, *Deregulation of ZIC Family Members in Oncogenesis* (Springer, 2018), pp. 329–338.
57. C. Garcia-Frigola, M. I. Carreres, C. Vegar, E. Herrera, Gene delivery into mouse retinal ganglion cells by in utero electroporation. *BMC Dev. Biol.* **7**, 103 (2007).
58. L. Y. Brown, A. H. Kottmann, S. Brown, Immunolocalization of Zic2 expression in the developing mouse forebrain. *Gene Expr. Patterns* **3**, 361–367 (2003).
59. A. Dobin, C. A. Davis, F. Schlesinger, J. Drenkow, C. Zaleski, S. Jha, P. Batut, M. Chaisson, T. R. Gingeras, STAR: Ultrafast universal RNA-seq aligner. *Bioinformatics* **29**, 15–21 (2013).
60. H. Li, B. Handsaker, A. Wysoker, T. Fennell, J. Ruan, N. Homer, G. Marth, G. Abecasis, R. Durbin; 1000 Genome Project Data Processing Subgroup, The Sequence Alignment/Map format and SAMtools. *Bioinformatics* **25**, 2078–2079 (2009).
61. S. Anders, P. T. Pyl, W. Huber, HTSeq—A Python framework to work with high-throughput sequencing data. *Bioinformatics* **31**, 166–169 (2015).
62. M. I. Love, W. Huber, S. Anders, Moderated estimation of fold change and dispersion for RNA-seq data with DESeq2. *Genome Biol.* **15**, 550 (2014).
63. W. Huber, V. J. Carey, R. Gentleman, S. Anders, M. Carlson, B. S. Carvalho, H. C. Bravo, S. Davis, L. Gatto, T. Girke, R. Gottardo, F. Hahne, K. D. Hansen, R. A. Irizarry, M. Lawrence, M. I. Love, J. MacDonald, V. Obenchain, A. K. Oleś, H. Pagès, A. Reyes, P. Shannon, G. K. Smyth, D. Tenenbaum, L. Waldron, M. Morgan, Orchestrating high-throughput genomic analysis with Bioconductor. *Nat. Methods* **12**, 115–121 (2015).
64. H. Thorvaldsdóttir, J. T. Robinson, J. P. Mesirov, Integrative Genomics Viewer (IGV): High-performance genomics data visualization and exploration. *Brief. Bioinform.* **14**, 178–192 (2013).
65. H. Mi, A. Muruganujan, X. Huang, D. Ebert, C. Mills, X. Guo, P. D. Thomas, Protocol update for large-scale genome and gene function analysis with the PANTHER classification system (v.14.0). *Nat. Protoc.* **14**, 703–721 (2019).
66. A. Subramanian, P. Tamayo, V. K. Mootha, S. Mukherjee, B. L. Ebert, M. A. Gillette, A. Paulovich, S. L. Pomeroy, T. R. Golub, E. S. Lander, J. P. Mesirov, Gene set enrichment analysis: A knowledge-based approach for interpreting genome-wide expression profiles. *Proc. Natl. Acad. Sci. U.S.A.* **102**, 15545–15550 (2005).

Acknowledgments: We thank Y. Coca and M. Herrera for technical assistance. We also thank P. Bovolenta for discussion and comments on the manuscript. **Funding:** The laboratory of E.H. is funded with the following grants: PID2019-110535GB-I00 from the National Grant Research Program, PROMETEO Program (2020/007) from Generalitat Valenciana, RAF-20191956 from the Ramón Areces Foundation, and ERC-2011-20101109. M.T.L.-C. is the recipient of an FPI fellowship from the National Grant Research Program. J.P.L.-A. research is supported by grants RYC-2015-18056 and RTI2018-102260-B-100 from MICINN co-financed by ERDF. A.B. research is supported by grant SAF2017-87928-R from MICINN co-financed by ERDF. We also acknowledge the financial support received from the "Severo Ochoa" Program for Centers of Excellence in R&D (SEV-2013-0317). **Author contributions:** C.M.-P. designed, performed, and analyzed most of the experiments. M.T.L.-C. and J.P.L.-A. have performed the computational analysis of RNA-seq data. D.B. performed in situ hybridizations and took care of the mice colonies. L.C.-D. performed some immunostainings. E.H. wrote the original draft and designed, conceived, and supervised the study. A.B. revised subsequent versions of the manuscript, helped with experimental design, and revisited critically the manuscript for important intellectual content. **Competing interests:** The authors declare that they have no competing interests. **Data and materials availability:** All data needed to evaluate the conclusions in the paper are present in the paper and/or the Supplementary Materials. Additional data related to this paper may be requested from the authors.

Submitted 16 October 2019
Accepted 30 September 2020
Published 13 November 2020
10.1126/sciadv.aaz8797

Citation: C. Morenilla-Palao, M. T. López-Cascales, J. P. López-Atalaya, D. Baeza, L. Calvo-Díaz, A. Barco, E. Herrera, A Zic2-regulated switch in a noncanonical Wnt/βcatenin pathway is essential for the formation of bilateral circuits. *Sci. Adv.* **6**, eaaz8797 (2020).